Virology 416 (2011) 32–41

Contents lists available at ScienceDirect

Virology

journal homepage: www.elsevier.com/locate/yviro

The parvoviral capsid controls an intracellular phase of infection essential for efficient killing of stepwise-transformed human fibroblasts

Justin Paglino [a], Peter Tattersall [a,b,*]

[a] Department of Laboratory Medicine, Yale University Medical School, 333 Cedar Street, New Haven, CT 06520, USA
[b] Department of Genetics, Yale University Medical School, 333 Cedar Street, New Haven, CT 06520, USA

ARTICLE INFO

Article history:
Received 15 February 2011
Returned to author for revision 1 April 2011
Accepted 25 April 2011
Available online 20 May 2011

Keywords:
LuIII
Minute Virus of Mice (MVM)
Parvovirus
Oncolytic
Oncolysis
Virotherapy
Tropism
VP2
qPCR
Stepwise transformation

ABSTRACT

Members of the rodent subgroup of the genus *Parvovirus* exhibit lytic replication and spread in many human tumor cells and are therefore attractive candidates for oncolytic virotherapy. However, the significant variation in tumor tropism observed for these viruses remains largely unexplained. We report here that LuIII kills BJ-ELR 'stepwise-transformed' human fibroblasts efficiently, while MVM does not. Using viral chimeras, we mapped this property to the LuIII capsid gene, VP2, which is necessary and sufficient to confer the killer phenotype on MVM. LuIII VP2 facilitates a post-entry, pre-DNA-amplification step early in the life cycle, suggesting the existence of an intracellular moiety whose efficient interaction with the incoming capsid shell is critical to infection. Thus targeting of human cancers of different tissue-type origins will require use of parvoviruses with capsids that effectively make this critical interaction.

Introduction

Members of the rodent subgroup of genus *Parvovirus*, including H-1, LuIII, and Minute Virus of Mice (MVM), are potential candidates for oncolytic virotherapy of human cancer for several reasons. Firstly, these viruses are naturally S-phase dependent, so that they preferentially target host cell populations that are proliferating, while sparing those that are not. The rodent parvoviruses are also markedly oncoselective, displaying enhanced fitness and toxicity in many human cancer cell lines compared to their untransformed counterparts, although they show variable tropism between tumor types (Chen et al., 1986; Chen et al., 1989; Cornelis et al., 2004; Dupont et al., 2000; Guetta et al., 1990; Legrand et al., 1992; Mousset et al., 1994; Rommelaere and Cornelis, 1991; Van Hille et al., 1989). They show potent oncosuppressive properties in many *in vivo* models, including syngeneic mouse tumor models and human xenografts transplanted into immunocompromised animals (Dupressoir et al., 1989; Faisst et al., 1998; Raykov et al., 2007; Rommelaere and Cornelis, 1991; Shi et al., 1997; Toolan, 1967; Toolan et al., 1982), and can also induce both curative and protective immune responses in some immunocompetent rodent tumor models (Guetta et al., 1986; Geletneky et al., 2010). Importantly for the prospective use of these agents in virotherapy of human cancer, there is no human disease associated with any known member of this genus (Dupont, 2003; Rommelaere and Cornelis, 1991; Siegl, 1984). Finally, the small diameter of these viruses, approximately 20–25 nm, may facilitate intra-tumoral virion spread (Everts and van der Poel, 2005; Wu et al., 2001), while their rugged virion structure would allow them to survive protracted storage with minimal loss of potency.

In the present study we first illustrate that different parvovirus species vary in their ability to grow in and kill particular cells, and that different transformed human cells are variably susceptibility to virus-mediated killing, thus presenting hurdles for the rational targeting of human cancers. In order to further study this aspect of parvoviral target cell specificity, we have examined parvoviral oncoselectivity in stepwise-transformed human cells. In this approach, normal primary human cells are rendered tumorigenic in nude mice by the sequential retroviral transduction of transforming genes (Hahn and Weinberg, 2002), potentially allowing dissection of the contributions of individual oncogenes to specific steps in the parvoviral life cycle. Here we use one of the best characterized of these model systems (Hahn et al., 1999) to show that untransformed human fibroblasts are resistant to killing by a panel of rodent sub-group parvoviruses, but that the fully-transformed derivative, while still resistant to most of these viruses, is efficiently killed by the orphan parvovirus LuIII. This property maps to the LuIII coat protein gene, the product of which plays a critical role early in the establishment of infection of these transformed cells.

* Corresponding author at: Department of Laboratory Medicine, Yale University Medical School, 333 Cedar Street, New Haven, CT 06520, USA. Fax: +1 203 688 7340.
E-mail address: peter.tattersall@yale.edu (P. Tattersall).

0042-6822/$ – see front matter © 2011 Elsevier Inc. All rights reserved.
doi:10.1016/j.virol.2011.04.015

Results

Rodent parvoviruses exhibit different host ranges in transformed human cells

In order to screen for the most effective virus:host cell combinations, we used a multi-well plate assay to monitor infection by a panel of five representative virus species that cluster phylogenetically with the rodent viruses within the genus *Parvovirus*. These include the prototype strain of the murine virus, MVMp, the two rat viruses H1 and H3 (the latter also known as Kilham Rat Virus), and two viruses of unknown animal origin, LuIII and TVX, originally isolated as contaminants of human cell lines (Hallauer et al., 1972). The viruses were grown in cell culture, purified and their genome concentrations determined by Southern blotting of alkaline gels probed with a conserved sequence oligonucleotide. Rapidly proliferating, sub-confluent monolayer cultures of cells in 24 well plates were infected at different input levels and stained for surviving cells 6 days post infection. This assay monitors several facets of viral infection, including acute killing at high multiplicity of infection (moi), as well as the virus' ability to proliferate and spread through the culture when infection is initiated at lower virus inputs. As shown in Fig. 1A, four of the viruses, MVMp, LuIII, H1 and H3 efficiently killed NB324K cells, while TVX had no detectable effect, even at high moi. In contrast, MVMp had no effect in HeLa cells, even at a high input level, while TVX completely destroyed the monolayer, even when infection was initiated at the lowest input multiplicity tested (32 genomes per cell, Fig. 1B). Since NB324K are papovavirus SV40-transformed newborn kidney cell line, whereas HeLa cells are derived from a papillomavirus-initiated cervical carcinoma, these two transformed human cell lines differ in many ways.

Complete stepwise oncogenic transformation of human fibroblasts dramatically enhances killing by parvovirus LuIII

Since it was unclear whether the differences in response to the parvovirus panel were due to the genetics of the host or tissue type, the nature of the transforming virus, or to stochastic differences that have arisen during transformation, we decided to examine the requirements for rodent parvovirus infection of transformed human cells in a more controlled fashion. To do this we tested the same panel of viruses for their ability to kill BJ primary human fibroblasts and their tumorigenic derivative, BJ-ELR, which were transformed by stepwise-addition of hTERT, the SV40 Early Region (SVER, which expresses both Large T Antigen (LT) and Small T Antigen (ST), and the activated proto-oncogene Ras^{V12} (Hahn et al., 1999). As shown in Fig. 1C, none of the five viruses had a detectable effect on the growth of the parental untransformed BJ cells at any of the input mois tested (up to 1000 genomes per cell). In contrast, two of the five viruses had pronounced effects on the survival of BJ-ELR monolayers (Fig. 1D). One of these, H1, only had observable effects at the highest input mois, but the other, LuIII, efficiently killed the majority of transformed cells down to an input of 64 genomes per cell, which represents a 16-fold lower initial moi than the maximum tested in this assay. Thus LuIII, and to a lesser extent by H1, are oncoselective for growth and killing in human fibroblasts since their infectivities are specifically enhanced by cellular alterations that drive oncogenesis. We also tested the lymphotropic strain of MVM, MVMi, for its ability to kill BJ-ELR, as well as three other MVM strains isolated as contaminants of commercial product streams (Garnick, 1996), but these all proved ineffective, indicating that BJ fibroblasts express a block to growth of MVM that is circumvented by LuIII.

Growth of MVM and LuIII are both enhanced by transformation, but only LuIII can expand effectively in transformed BJ cells

To better understand the phenotypes of MVMp and LuIII observed in the killing assay, we used an expansion assay, which measures the

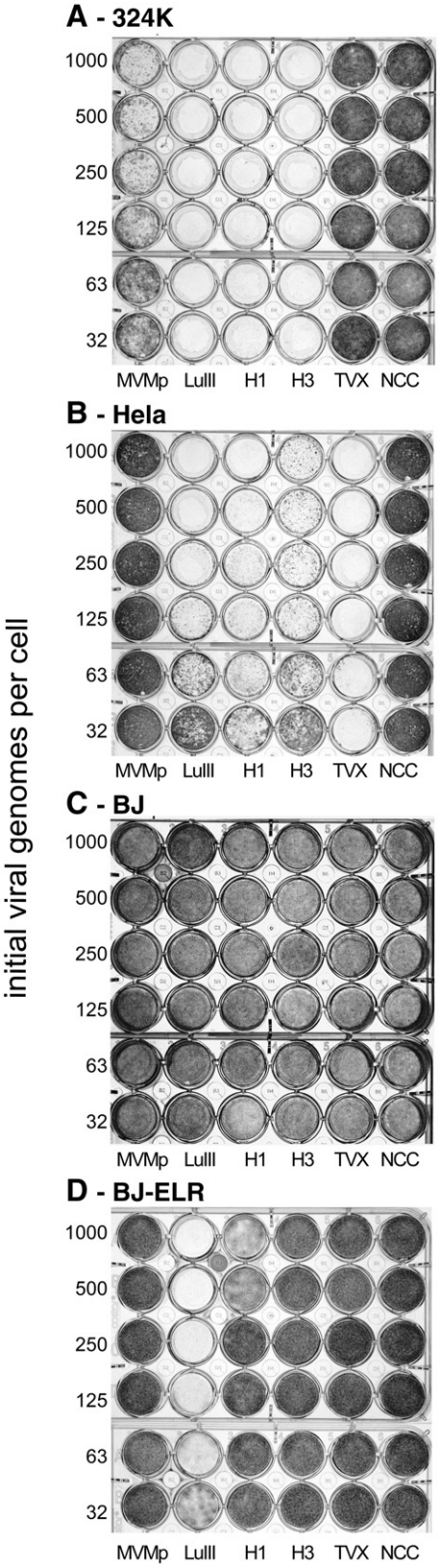

Fig. 1. Killing of transformed and normal human cells by a panel of five parvoviruses. Panel A: SV40-transformed new-born human kidney cells, NB324K, were seeded in 24-well plates at low density and infected at different multiplicities with genome-titered purified viral stocks of representative isolates of different species of *Parvovirus*, as indicated. Monolayers were incubated, fixed and stained as described in Materials and methods. The right-hand column represents the normal cell control (NCC). Panel B: HeLa cervical carcinoma cells; Panel C: BJ human fibroblasts; and Panel D: stepwise-transformed BJ-ELR (BJ + hTERT + SVER (LT + ST) + Ras) cells, respectively, were analyzed for viral killing as described for panel A.

ability of each virus to spread through a culture of growing cells. This assay compares the fraction of cells that are positive for viral NS1 antigen at 24 and 72 hours post infection (hpi) in rapidly growing cultures initially infected at low moi. As shown in Fig. 2A, the expansion index of MVM in BJ cells was significantly less than one (0.3 ± 0.04), indicating that the percentage of cells infected decreased over time, consistent with little or no progeny virus production. By comparison ($p<0.005$), an expansion index of approximately 1.0 (1.4 ± 0.7) for MVM in BJ-ELR suggested it was able to produce sufficient progeny to maintain a "balanced" or "persistent" infection, in which the percentage of cells infected remains relatively unchanged over time as the culture itself expands. In fact we found this to be the case, and were able to passage an MVM-infected culture of BJ-ELR for over 20 population doublings while the percentage of infected cells remained between 0% and 2% (data not shown). Thus MVMp does exhibit modest oncoselectivity in this assay, but even complete transformation does not remove all blocks to viral expansion. In contrast, LuIII has an expansion index of 1.1 ± 0.07 even in BJ cells, showing that it is better adapted to untransformed human fibroblasts than MVMp ($p<0.005$). Moreover, the addition of hTERT, SVER, and Ras raises the expansion index for LuIII by a further 50-fold (59 ± 12), clearly demonstrating that oncogenic transformation of human fibroblasts enables LuIII to expand efficiently through the culture. As might be expected, the expansion indices for all four virus:cell pairs correlate well with the previously observed efficiencies of killing, since an expansion index significantly greater than one would be necessary to kill an entire culture of growing cells initially infected at a low moi.

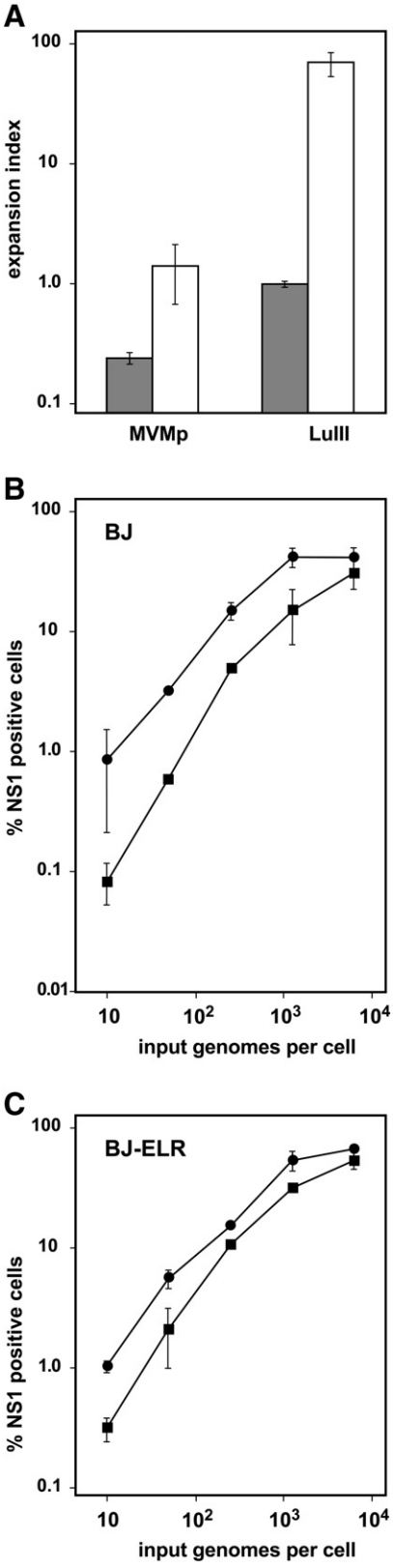

The expansion data show that both viruses are oncoselective to a certain degree in this model system, but that MVMp is disadvantaged compared to LuIII in BJ cells, regardless of their transformation status. To ask whether early viral life cycle events are responsible for these differences, we compared their initiation efficiencies in an assay that measures the overall efficacy of the early steps in infection, including binding, entry, endosomal escape, nuclear trafficking, uncoating, and NS1 expression. As seen in Fig. 2, while initiation frequencies for LuIII appeared very similar in both cell types, we observed a 2.9-fold (± 1.5) initiation advantage for LuIII over MVM in BJ (Fig. 2B), and 1.7-fold (± 0.5) advantage for LuIII in BJ-ELR (Fig. 2C). Thus, LuIII exhibits a distinct advantage over MVM in initiating infection of both normal and transformed lines, but whether this difference alone is enough to explain the dramatic disparity between the killing effects of the two viruses in BJ-ELR cells required further examination.

The VP2 ORF of LuIII promotes efficient killing of BJ-ELR by an MVM-LuIII chimera

Next we used viral genomic chimeras to ask whether there was a single region of LuIII that could confer its killing phenotype on MVMp. These recombinants shuffled four major sections of the genome, the left-hand hairpin, the NS coding region, the VP coding region, and the right-hand hairpin, between LuIII and MVMp as diagrammed in Fig. 3A, where M or L in the virus name denotes the origin of each segment in order along the genome. In addition, we generated LuCap, which contains just the VP2 gene of LuIII in the MVMp backbone. Fig. 3B shows the results of killing assays performed in BJ-ELR with these viruses. The MLLM recombinant showed the same killing efficiency as LuIII, indicating that the hairpins of LuIII confer no advantage over those of MVM in this cell line. The MMLM chimera was 3–4 fold less efficient at killing than LuIII,

Fig. 2. Infection parameters of MVM and LuIII in BJ and BJ-ELR. Panel A: The ability of each virus to expand within each cell line was measured in spot slides cultures of BJ or BJ-ELR, infected at low multiplicity with MVM or LuIII. Parallel slides were fixed at 24 hpi and 72 hpi and assessed for NS1 expression by fluorescent antibody staining. The fraction of NS1-positive cells at 72 h was divided by the fraction positive at 24 h to calculate the expansion index for MVM and LuIII in BJ cells (light gray bars) and BJ-ELR cells (unfilled bars). Data points represent average values from two independent experiments and error bars represent a single standard deviation in either direction. Initiation efficiencies for MVM (–■–) and LuIII (–●–) are shown in Panel B for BJ cells and in Panel C for BJ-LER cells. The cells were infected over a range of multiplicities with MVM or LuIII, incubated in medium with neuraminidase until 24 hpi, and then fixed and assayed for NS1 expression by immunofluorescence microscopy. Data points represent the average value from two independent experiments, and error bars represent a single standard deviation in each direction.

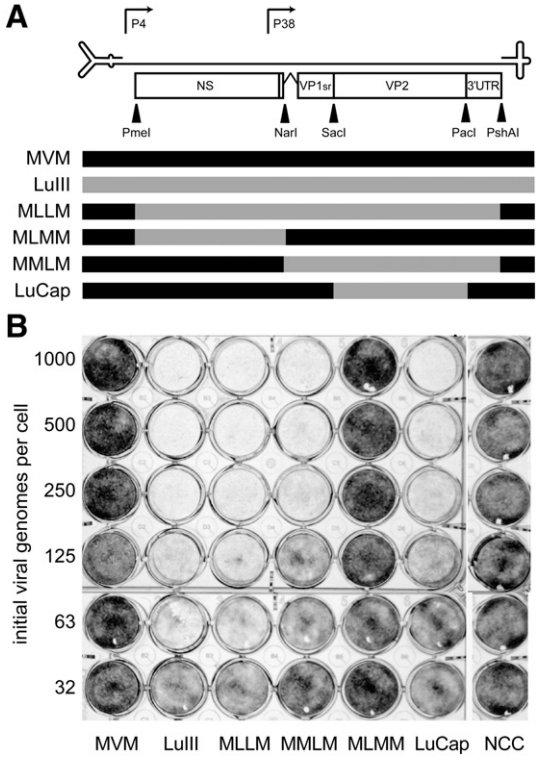

Fig. 3. Killing of BJ-ELR by chimeric viruses. Panel A shows a map of genomic features common to MVM and LuIII, showing hairpins, promoters, major ORFs, and the 3′ UTR. The location of restriction sites used to generate chimeras between LuIII and MVM are indicated. MVM, LuIII, and chimeras MLLM, MLMM, MMLM, and LuCap are diagrammed to indicate the origin of each section of the genome. Panel B shows killing assays for the chimeras and their parents in BJ-ELR cells, performed as described for Fig. 1.

yet retained the ability to kill the majority of BJ-ELR at 250 genomes per cell; an input that was determined by initiation assays (not shown) to result in the initial infection of ~10% of BJ-ELR cells. These findings, together with an observed expansion index for MMLM of 50 (not shown), support the contention that the region spanning the VP gene cassette is sufficient for productive infection of BJ-ELR cultures. The further 3–4 fold increase in efficiency seen for MLLM suggests that the NS region of LuIII provides an incremental advantage over that of MVM in BJ-ELR, but that this advantage is not necessary for productive and lytic growth. Conversely, the NS-spanning region of LuIII alone is not sufficient to confer the expansion phenotype in BJ-ELR, as demonstrated by the MLMM virus, which was indistinguishable in this assay from MVMp (Fig. 3B).

As shown in Fig. 3A, the VP gene in MMLM includes not only the LuIII VP2 gene, but also the LuIII VP1-specific region, which, in MVM, is responsible for several essential functions in viral entry (Farr et al., 2005). In addition this region contains the 3′ UTR, for which no distinct function has yet been established. However, these regions of LuIII do not significantly contribute to expansion in BJ-ELR cells, since the LuCap chimera exhibits the same killing phenotype as MMLM (Fig. 3B), indicating that the LuIII VP2 ORF alone is sufficient to overcome the significant block to growth encountered by MVMp in these transformed cells. This finding allowed us to use many of the genetic and serological tools that we had already developed for MVM to analyze the role of the LuIII VP2 in dramatically facilitating parvoviral infection of these stepwise transformed human fibroblasts.

Use of differential qPCR to detect small differences in viral fitness

Next we attempted to measure the contribution of LuIII VP2 to initial event(s) in the viral life cycle by comparing MVMp with LuCap using the initiation assay. While this assay confirmed that LuCap had an advantage over MVMp in BJ-ELR, the difference was relatively minor, as observed previously for the parental viruses (Fig. 2). This raised the concern that errors inherent in side-by-side comparison of separate infections might be confounding, and suggested that an internally controlled method of comparing the two viruses would be required to test their relative fitness in a sufficiently exact way. The strategy we adopted was to co-infect cells with an equimolar mixture of two viruses containing differently marked genomes, and then compare the ratios of each co-infecting genome at several time points by differential qPCR. Determining the ratio of the two genomes in any particular sample reduces inaccuracies, since both would be subject equally to any errors in dilution, processing, or sampling for PCR, as well as differences between individual infected cell cultures.

To allow multiplex qPCR measurements of genome ratio, we constructed LuAlt, a phenocopy of LuCap with eight silent mutations in its MVMp-derived NS1 ORF, as shown in Fig. 4A. LuAlt was designed to serve as a competitor for either MVMp, in experimental co-infections, or LuCap in control co-infections. In this differential assay, the mutated region of LuAlt binds a VIC fluorophore-labeled probe termed “alternate,” whereas the wildtype sequence in this region of MVMp or LuCap binds a FAM-labeled probe, designated “standard.” Using common outside primers and real-time qPCR, we validated the assay by measuring LuCap genomes alone, LuAlt genomes alone, or equimolar mixtures of LuCap and LuAlt genomes. Fig. 4B and C shows the strong correlation ($r = -0.999$ in both cases) between genomes per reaction and Ct observed for both probes over a five $\log_{10}$ range, from 10^3 to 10^8 genomes per reaction. Both probes were highly specific, as each failed to generate signal above the Ct threshold after 45 cycles in a reaction with 10^8 copies of the non-targeted sequence.

To check that the overall replicative efficiency of LuAlt was the same as LuCap, we performed a co-infection over multiple rounds of viral growth, in order to allow any fitness difference between the co-infecting/competing viruses to compound over time. Accordingly, low density BJ-ELR cultures were infected with an equimolar mixture of LuCap and LuAlt, or an equimolar mixture of MVM and LuAlt, representing a total input moi of 40 genomes per cell, sufficient to infect approximately 1% of cells initially, and passaged as described in the Materials and methods. After each of two passages, the relative genome concentrations were determined by qPCR and expressed as “Fraction Standard” (F_s), calculated as described in Materials and methods. As shown in Fig. 4D, there was no significant change in this parameter over one or two passages for co-infections of Lu-Cap and LuAlt. This result indicated that the eight single base differences between the two genomes conferred no particular advantage on either virus over 6 days of multiple-cycle growth, allowing us to use co-infections with MVMp and LuAlt to explore the difference in fitness between viruses conferred by the VP2-ORF alone. As shown in Fig. 4D, LuAlt extensively outgrew MVM after one multiple-cycle passage, as would be expected from the killing assay and expansion data. Specifically, after the first passage the MVMp standard virus represented just ~9% of progeny virus, and after the second passage only 0.5%, indicating that the VP2 ORF of LuIII confers a significant advantage for some aspect(s) of viral replication in BJ-ELR cells.

The LuIII capsid does not enhance receptor binding, entry, or occlusion in BJ-ELR

The multiplex qPCR assay also provided a sensitive tool for exploring early steps in the life cycle that might potentially be enhanced by delivering the viral genome in LuIII VP2 capsids. For this BJ-ELR were co-infected at high multiplicity with either of the two mixed inocula, LuCap (standard) plus LuAlt, or MVMp (standard) plus LuAlt, and cells and medium harvested at 4 and 6 hpi. Samples were then digested with micrococcal nuclease to remove unencapsidated viral DNA, and analyzed by qPCR. Fig. 5A shows F_s values for input

virions, unadsorbed virions, and cell-associated virions, measured at 4 hpi. As expected, the F_s for the LuCap versus LuAlt control co-infection remained unchanged from the input value in both the cell extract and the medium. Significantly, the same result was observed for the MVMp versus LuAlt combination. Because there was no significant decrease seen in F_s for either the cell extract or the post-adsorption medium, we conclude that genomes encapsidated in either VP2 shell become cell-associated with the same efficiency over the 4-h incubation, during which time approximately 25% of each virus inoculum attached to the cells.

Following the initial incubation step, a parallel culture was incubated for two more hours in fresh medium containing neuraminidase, allowing time for viral receptor cleavage and the removal of surface-bound virions. Virus that remained cell-associated at 6 hpi, following neuraminidase treatment, was characterized as "occluded," and comprised the sum of virions inside endosomes, those that had escaped from that compartment into the cytosol and were en route to the nucleus, and those in the nucleus. Occluded virus at 6 hpi represented approximately 85% of the virus that was cell-associated at 4 hpi, suggesting that most cell-associated virus had already been internalized by the cell at 4 hpi, and also that little of this was recycled back on to the cell surface during the next 2 h. As expected, the F_s for the LuCap plus LuAlt control co-infection remained unchanged from the input value in both the cell extract and the medium, as shown in Fig. 5B. Once again, however, we saw a similar result for the MVMp plus LuAlt co-infection. Because there was still no decline in F_s in the cell extract or increase in F_s in the medium by 6 hpi, we conclude that the kinetics of occlusion are essentially identical for genomes contained in capsids of MVM or LuIII origin.

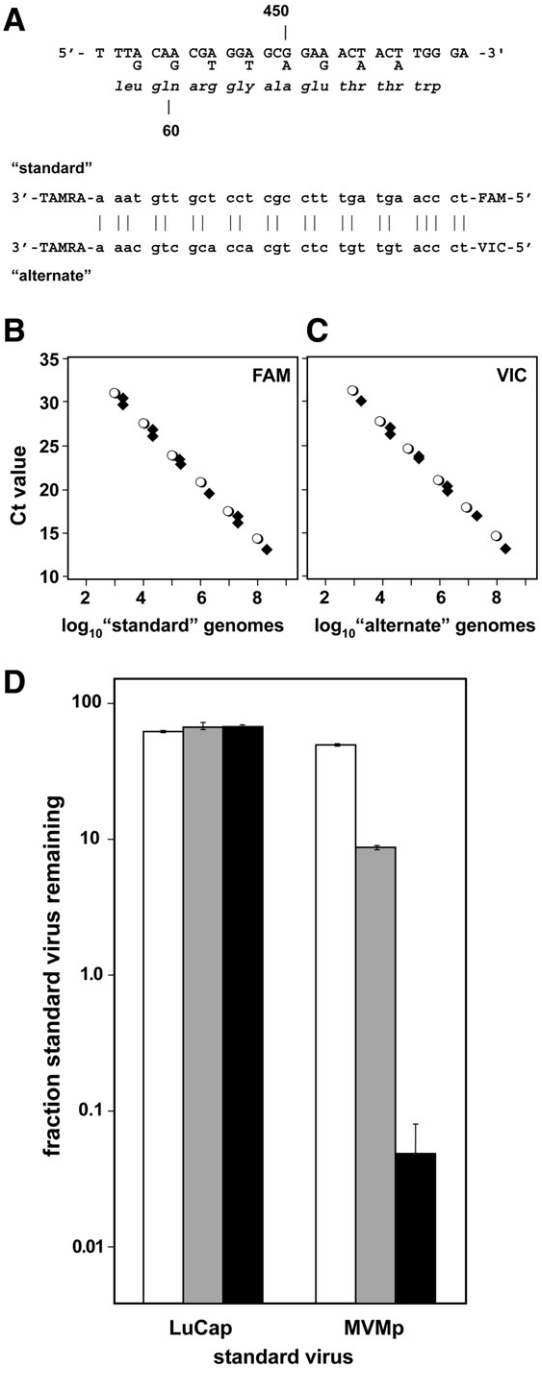

Fig. 4. Relative fitness analysis using differential qPCR. Panel A. Positive strand nucleotides 436–459 within the NS gene of wildtype MVMp, and thus of LuCap (see Fig. 3), are shown above the eight single base changes introduced to create LuCap-Alt. Oligonucleotide probes for discriminating between these two "standard" and "alternate" sequences are diagrammed, labeled with FAM and VIC fluorophores, respectively. Both probes bear the TAMRA quencher at their 3′ ends, which is separated from the fluorophore at the 5' end of bound probe by the endonuclease activity of the TaqMan® polymerase during the PCR reaction. Panels B and C show quantitation of standard and alternate genomes, respectively, over a range of concentrations, as indicated, using Taq-Man real-time PCR, either alone (○) or in an equimolar mixture with the other genome type (♦). Ct value represents the PCR cycle at which fluorescent signal from the fluorophore crossed a set threshold value. Panel D shows relative fitness determinations for LuCap-Alt versus either LuCap or MVMp standard virions. BJ-ELR were co-infected at low multiplicity with either LuCap or MVM mixed with LuCap-Alt virus at an approximately equimolar ratio, as determined by Southern blot analysis. Initial F_s values were determined from a sample of each inoculum by qPCR (unfilled bars). After 72 h of multi-step co-culture, total progeny virus was analyzed by qPCR, as described in Materials and methods, and the F_s for the first passage determined (gray bars). These samples were then used to infect another set of cultures, which were processed as before, and the F_s after the second passage calculated (black bars). Data points for F_s represent the average of two separate plates, each one assayed in duplicate, and error bars represent one standard deviation in either direction.

The LuIII VP2 ORF facilitates a step prior to viral genome amplification

We next wished to examine whether LuIII VP2 confers an advantage at an early post-entry step of the viral life cycle, such as escape from the endosome, trafficking to the nucleus or uncoating. However, the high particle-to-infectivity ratios required for these experiments and the low efficiency of endosomal escape rendered it impossible for us to identify productive routes of infection using the qPCR assay. Accordingly, we restricted our analysis of these events to monitoring subsequent DNA amplification, using differential qPCR to measure viral DNA replication during a co-infection conducted under one step growth conditions. Low molecular weight DNA was extracted from co-infected cells at 6, 24 and 48 hpi using the method of Hirt (Hirt, 1967), which isolates replicative form (RF) DNA molecules and releases single-stranded genomes from progeny virions. For the 24 and 48 hpi samples, which contain significant amounts of RF as well as progeny DNA, we took the further step of individually separating and isolating the duplex 5 kbp monomer and 10 kbp dimer RFs by agarose gel electrophoresis and gel extraction. The Southern blot of a parallel agarose gel (Fig. 6A) shows these predominant 5 kb and 10 kb viral RF DNA species in the 24- and 48-h Hirt extracts. A longer exposure of this blot also revealed a single-stranded progeny form that co-migrated with single-stranded DNA from occluded input genomes in the 6-h Hirt extract. F_s values were determined for the 6-h Hirt extract, as well as for the 5 and 10 kb gel extracts at 24 hpi and 48 hpi, and results are shown in Fig. 6B.

As expected, no significant change in F_s was observed in any sample from the LuCap vs LuAlt co-infection. In contrast, MVM sequences represented only ~10% of 5Kb and 10Kb forms in the MVMp plus LuAlt co-infection extracted at 24 hpi, down from 50% of occluded genomes in the 6 hpi extract. The under-representation of

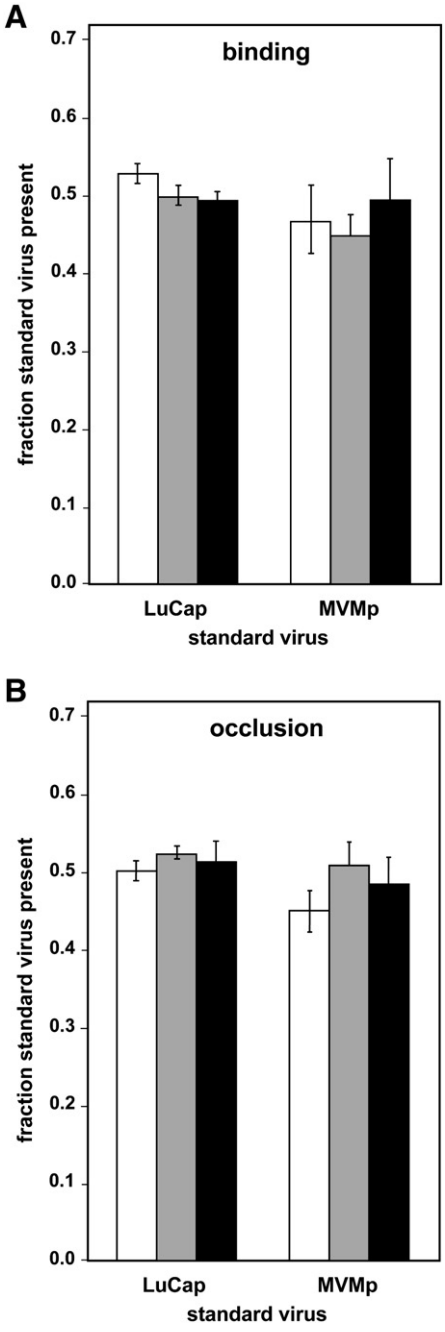

Fig. 5. Binding and entry/occlusion. BJ-ELR were co-infected at high multiplicity with an equimolar mix of LuCap-Alt and standard LuCap or MVMp viruses. Panel A shows initial F_s values determined from the inoculum as described in Fig. 4 (unfilled bars). After 4r h of incubation, unattached (gray bars) and cell-associated virions (black bars) were isolated as described in Materials and methods, and their F_s values determined by differential qPCR. At the same time, the medium on a set of parallel plates was replaced with medium containing neuraminidase, to remove viral receptors, and cultures incubated for an additional 2 h. Panel B shows F_s values determined for detached or recycled encapsulated genomes (gray bars) and cell-associated, or occluded, virions (black bars), at 6 hpi. Data points represent an average value from two separate plates, and error bars represent one standard deviation in either direction.

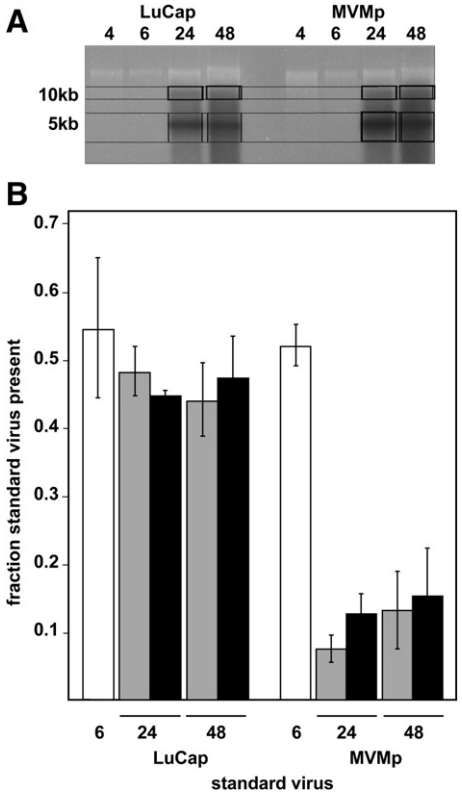

Fig. 6. DNA replication in coinfected cells. BJ-ELR were co-infected at high multiplicity with equimolar mixtures of LuCap-Alt with either LuCap and MVM standard viruses, as before. Cell samples from 4, 6, 24, and 48 hpi were processed for small molecular weight DNA by Hirt extract as described in Materials and methods, where neuraminidase was present from 4 h onwards. Panel A shows an image of the ethidium stained gel overlayed with the autoradiograph of a Southern blot of the same gel probed for viral DNA. In the lanes containing the 24 and 48 h samples, boxes represent the regions of a parallel gel from which DNA was extracted. Panel B shows F_s values determined by qPCR for 6 h Hirt extract, tested directly (unfilled bars), 5 kb (gray bars) or 10 kb species (black bars), extracted from gel slices for 24 or 48 h samples, as indicated. Data points represent the average of at least three qPCR measurements, and error bars indicate one standard deviation in either direction.

MVM sequences in the RF population at a single time point could reflect either a block between occlusion and initiation of MVM DNA replication, or slower MVMp genome amplification, compared to that of LuAlt. To look for differences in kinetics of DNA amplification between the two viruses, we compared the F_s values for 5Kb and 10Kb RF at 24 and 48 hpi. No significant decrease in F_s value for either RF species was observed over that time period, indicating that, once initiated, DNA amplification continues with the same kinetics for both viruses. Thus it appears likely that the diminished F_s observed at 24 h is due to a VP2-dependent difference in the two viral life cycles that occurs at or before the onset of DNA amplification, either at the stage of endosomal escape, nuclear trafficking, virion uncoating, early gene expression, or the initiation of effective replication complexes.

LuIII VP2 confers no significant advantage for progeny single-stranded DNA synthesis or post-replication events

The parvoviral VP2 N-terminus is known to be involved in nuclear export in some cell lines (Maroto et al., 2004), and certainly the efficiency of capsid assembly, packaging and release from the cell might differ between different capsid proteins, providing additional potential advantages for LuIII VP2 later in the lifecycle. In order to test for differences in these later events between the two viruses, we measured F_s for encapsidated progeny genomes at 24 and 48 h, both in cell extracts and in the medium. Fig. 7 shows that 24 h after an equimolar MVM plus LuAlt co-infection, approximately 10% of progeny genomes are MVM, both in the cells and in the medium. These F_s values are not significantly different from those measured for viral RF at the same time point, indicating that there is no difference in the kinetics of progeny genome packaging attributable to the disparate VP2s. This is corroborated by the finding that at 48 h there is no diminution in F_s from that seen at 24 h, showing that indeed

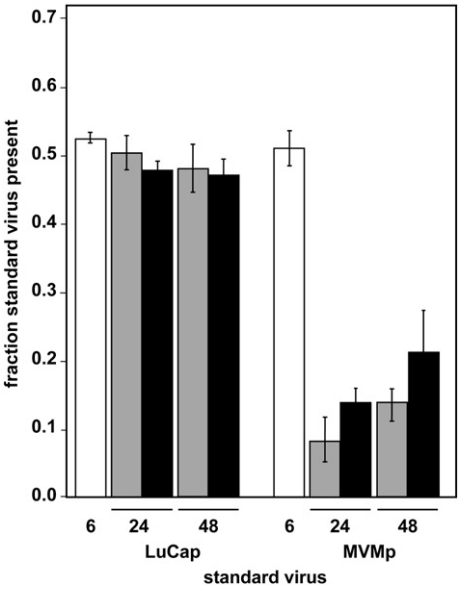

Fig. 7. Progeny production and export. BJ-ELR were co-infected at high multiplicity with equimolar mixtures of LuCap-Alt with either LuCap and MVM standard viruses, as before. Cells and medium were harvested at 6 hpi, 24 hpi, and 48 hpi, processed and analyzed by qPCR to determine F_s values for encapsidated genomes for the 6-h occluded virus sample (unfilled bars), and for either cell-associated progeny virus (gray bars), or progeny virions released into the medium (black bars), at 24 or 48 hpi, as indicated. Data points represent the average values from at least two separate plates, and error bars represent one standard deviation in either direction.

MVM and LuAlt progeny virions accumulate at the same rate. Additionally, since we did not observe any relative increase in F_s for progeny in the cell extract versus progeny in the medium, either at 24 or 48 h, we conclude that LuIII VP2 does not confer an advantage for virion export from the cell. The possibility also exists that MVMp genomes could be trans-encapsidated into LuIII VP2 capsids in co-infected cells, thereby masking a possible defect in downstream packaging or export for MVMp VP2 capsids. However, based on the initiation data shown in Fig. 2B, we estimate that a significant majority of infected cells were singly-infected, rather than co-infected, at the multiplicities used. Thus it is unlikely that trans-encapsidation could obscure a packaging or export defect of any magnitude.

Discussion

Stepwise models of human cellular oncogenic transformation, such as that originally described by Hahn and Weinberg (2002) offer clear advantages for studying parvoviral oncoselectivity. The transformed human cells are directly derived from their normal precursor by defined steps, and each of these can be studied individually for their contribution to parvoviral growth. However, initial efforts to study the oncoselectivity of MVM in this cell system were confounded by the inefficiency of MVMp replication and killing in the stepwise transformed cells, which was surprising since this virus grows well in a variety of human cell lines, particularly in 324 K, newborn kidney cells transformed with SV40. The study of adeno-associated virus (AAV) vectors over the past decade or more has demonstrated that different AAV serotypes showed dramatically different abilities to transduce therapeutic or reporter genes into cells of different human or murine tissue types (Arruda and Xiao, 2007; Van Vliet et al., 2008). In the family *Parvoviridae*, serotype is a major defining component of species, so that different serotypes within the genus *Dependovirus* are considered separate species, and isolates of the same species within the genus *Parvovirus* are highly related serologically, but antigenically quite distinct from isolates of other species (Tattersall et al., 2005). This consideration prompted us to screen strains derived from different *Parvovirus* species for their ability to expand in and kill BJ-ELR cultures, resulting in the identification of LuIII as the oncolytic virus of choice for these cells.

The advantage of LuIII over MVMp is observed in both normal and transformed human fibroblasts, suggesting that the underlying mechanism is a consequence of the differentiation phenotype of the host cell, rather than LuIII being intrinsically more oncoselective than MVM. The differential qPCR approach provided accurate comparison of the efficiency with which each virus completes certain individual steps in the infectious process, and allowed us to narrow down the LuIII advantage to a step between endosomal escape and the initiation of viral DNA replication. This result resembles a cell culture model of parvoviral tissue tropism that our laboratory has studied for several years. MVMp and MVMi, two strains of the same *Parvovirus* species, are reciprocally restricted for growth in each other's host cell types, fibroblasts and T-lymphocytes, respectively (Tattersall and Bratton, 1983). In fibroblasts, MVMi initiates NS1 expression with 5–10 fold lower efficiency than MVMp, indicative of an early life cycle block (Ball-Goodrich and Tattersall, 1992) and MVMp is similarly restricted in lymphocytes. MVMp and MVMi, however, reciprocally compete for binding to receptors on the surface of each other's host cell (Spalholz and Tattersall, 1983), suggesting that the point of restriction is at a subsequent, probably intracellular, step. Mapping of the fibrotropic determinant through the use of inter-strain recombinants identified two amino acid substitutions in the VP2 of MVMi, at positions 317 and 321, are sufficient to increase this strain's infectivity in fibroblasts to that of MVMp (Gardiner and Tattersall, 1988b), which in turn allows overall replication in fibroblasts to reach an level of efficiency approaching that of MVMp (Ball-Goodrich and Tattersall, 1992). Subsequently, several pairs of amino acid changes that coordinately switched the tropism of MVMi were mapped to residues lining the depression at the capsid two-fold symmetry axis (Agbandje-McKenna et al., 1998), a region that has been dubbed the 'allotropic determinant', and that corresponds to the capsid glycan-binding pocket (Nam et al., 2006).

Previsani et al. (1997) reported that input genomes of MVMi and MVMp3, an MVMi chimera carrying the MVMp allotropic determinant, reached the nuclear compartment of EL4 T-lymphocytes with similar efficiency and kinetics to MVMp, but that MVMp3 subsequently exhibited a major defect in the timing and extent of viral DNA amplification. Later steps in the viral life cycle were not affected by the origin of the allotropic determinant, since transfection of infectious clones of either MVMp or MVMi into either host cell resulted in equivalent single round infectious cycles (Gardiner and Tattersall, 1988a; Previsani et al., 1997), leading to the suggestion that the allotropic determinant region of the capsid interacts with an intracellular factor that catalyzes an essential early event in the viral life cycle, such as endosomal escape, nuclear trafficking, or uncoating, although the finding of similar kinetics in nuclear transport favor a post-nuclear-entry step, perhaps uncoating. The robust reciprocal blocks to growth of MVM strains in each other's host cell therefore appears to mirror the block to MVMp capsid-mediated infection of stepwise transformed human fibroblasts we report here. The molecular mechanism controlling tropism in both cases is unclear, but at least in the case of LuCap and MVM, there appears to be competition between viruses in cells co-infected at high input multiplicity, to the specific disadvantage of MVMp (data not shown), suggesting that the VP2 of LuIII has a higher affinity than that of MVMp for an unidentified intracellular factor, or "co-receptor." In this scenario, the interaction of the capsid with this co-receptor might take place in the endosome, the cytosol, or the nucleus, and would play an essential role in a critical local event. Significantly, the NS1 expression advantage for LuIII over MVMp is only 1.7-fold in BJ-ELR (Fig. 2C), whereas LuAlt replicative DNA is approximately 5-fold more abundant than is that of MVMp at 24 and 48 hpi (Fig. 6B). This might argue in favor of the critical step enhanced by LuIII VP2

occurring after gene expression, but before DNA replication. Further experiments exploring these early stages of the infectious process will be required to exact step(s) at which the LuIII VP2 advantage is executed.

An alternative explanation for the advantage conferred by the LuIII capsid is that a nucleotide element within the VP2 gene determines tropism, rather than the gene product itself. Although this possibility is not formally ruled out by the data presented here, it seems unlikely since trans-encapsidation experiments performed by others have identified the capsid protein proper as determinative of parvoviral tropism in other human cell types (Wrzesinski et al., 2003; Maxwell et al., 1995).

The sequence of LuIII VP2 differs from that of MVMp at 170 amino acid residues, representing ~30% of the protein. Approximately one third of these differences are conservative and, by comparison with the known structure of MVMp, the great majority of them are predicted to be on the viral surface. Interestingly, homology drops to less than 50% across the two regions that form a cleft at the icosahedral two-fold axes to which the MVM allotropic determinant maps. Analysis of further intragenic VP2 recombinants will be required to establish if structural features within this two-fold cleft are also responsible for the capsid-mediated restriction described here. Nam et al. (2006) have suggested that differences in glycan-binding specificity of the pocket at the capsid 2-fold cleft define the allotropic phenotypes of MVMp and MVMi. Such a mechanism may also underlie the differential target cell specificity reported here, however differences between the glycan-binding profiles of MVMp and LuIII remain to be explored, as does the putative role of interactions between the capsid and cellular glycans in determining the efficiency of establishing infection in human cells by these rodent parvoviruses.

Infection by both MVMp and LuIII is augmented by stepwise oncogenic transformation, consistent with multiple previous demonstrations of parvoviral oncoselectivity. That oncogenes hTERT, LT, ST, and Ras collectively enhance the parvoviral lifecycle opens the possibility of using this, or similar models, to explore the contribution of individual oncogenes to parvoviral growth in human cells. However, despite the facilitating effect of stepwise transformation for both LuIII and MVMp, the latter remains substantially blocked for efficient growth in fully transformed human BJ fibroblasts. We postulate that the characteristic enhancement of parvoviral growth by transformation can be effectively "trumped" by the target cell's differentiation phenotype. Effective targeting of human tumors will, therefore, depend on selection of a VP2 for the vector that is appropriate for targeting the tissue of origin for each particular tumor. Thus, future attempts to identify appropriate parvoviral capsids for different human tumors will likely parallel the many previous studies that have revealed a pivotal role for AAV serotype in the effective targeting of AAV-based gene therapy vectors (Arruda and Xiao, 2007; Van Vliet et al., 2008).

Materials and methods

Cells

Normal primary diploid human foreskin fibroblasts BJ were obtained from the ATCC (Manassas, VA). BJ-ELR (BJ + TERT, Ras, SVER) were the kind gift of Dr. Robert Weinberg (Whitehead Institute for Biomedical Research). All cells were grown in Dulbecco's Modified Eagle's Medium (DMEM) containing 10% fetal bovine serum, non-essential amino acids, sodium pyruvate, glutamine, penicillin, and streptomycin.

Infection initiation assay

4000 BJ or BJ-ELR were seeded on Teflon-coated glass spot-slides, incubated overnight at 37 °C, and infected with virus at the indicated inputs for 2 h. The inoculum was then exchanged for growth medium containing 0.1 μg/ml neuraminidase. Slides were fixed and stained for NS1 at 24 hpi, as described previously (Farr and Tattersall, 2004).

Expansion assay

2500 BJ or BJ-ELR were seeded on glass spots on Teflon coated spot-slides, incubated overnight at 37 °C, and infected at 100 genomes per cell for 2 h at 37 °C. The inoculum was then replaced with 100 μL of growth medium and incubated at 37 °C. Separate slides were fixed and stained for NS1 at 24 and 72 hpi, as previously described (Farr and Tattersall, 2004).

Viral constructs

pdBMVp, an infectious clone of MVMp, was described previously (Cotmore and Tattersall, 1992). pLU1Nde, an infectious clone of LuIII, and pMLLM were described previously (Cotmore and Tattersall, 2005). pMMLM was generated by exchanging the 2954 nt NarI–AatII fragment of pdBMVp for that of pMLLM. pMLMM was generated by exchanging the 2942 nt NarI–AatII fragment of pMLLM for that of pdBMVp.

To generate pSac-Pac, the precursor to pLuCap, a silent PacI site was engineered at the end of the VP2ORF of pdBMVp-Sac, a previously constructed derivative of pdBMVp with a silent SacI site at the beginning of the VP2 ORF (Farr et al., 2006). To generate pLuCap, the VP2 ORF of LuIII was PCR amplified with mutagenic primers introducing a PacI site (LUPAC 5′-G C A T A G T T A A T T A A T A A G T G T T T C T A G C-3′) at the end of the VP2 ORF and a SacI site (LUSAC2 5′-G C T G C G C A G C A G A G C T C T C A G A C A A T-3′) at the beginning of the VP2 ORF (restriction sites underlined). The PCR product was digested with SacI and PacI, gel-purified, and cloned into pre-digested pdBMVp-Sac-Pac, and the entire insert sequenced in both directions. pLuAlt was generated using two-step PCR mutagenesis, using overlapping central primers to introduce eight sequential silent third-position codon mutations in the NS1 ORF of pLuCap, as described in Fig. 4A.

Killing assay

10,000 cells were seeded in a volume of 800 μL per well in 24-well plates and incubated overnight. 200 μL of inoculum of the appropriate dilution was then added to each well. After 6 days of incubation at 37 °C, the monolayers were visualized by staining with Leishman's solution. Images were processed, as a group, in Adobe Photoshop.

Real-time multiplex qPCR

Primers and probes for qPCR were designed using Primer Express® software and employed TaqMan® technology (Applied Biosystems, Foster City, CA). Fluorescent probes were purchased from Applied Biosystems. "Standard" and "Alternate" probe designs are illustrated in Fig. 4A. Probes were added to each reaction at 250 nM. PCR amplification was accomplished with outside primers OKFW 5′-G C A G G A G G A C G A G C T G A A A T-3′ and OKRV 5′-C C C A T T C C A T G T C C T C G C-3′, each at 900 nM. PCR reactions were performed and analyzed using the Applied Biosystems PRISM® 7900 Sequence Detection System instrument and software, in accordance with the manufacturer's recommendations. Standards, consisting of serial 10-fold dilutions equimolar mixtures of "standard" and "alternate" tagged genomes in plasmid form, ranging from 10^3 to 10^8 genomes per reaction, were included in duplicate in each run of PCR, and separate standard curves were generated for FAM and VIC fluorescence. All samples were measured in duplicate. The "Fraction Standard" (F_s), is the fraction of total genomes in a sample that are standard, as determined by qPCR, and calculated as follows: $F_s = [\text{Std}]/([\text{Std}] + [\text{Alt}])$ where [Std] = measured concentration of standard genomes, and [Alt] = measured concentration of alternate genomes.

Measurement of encapsidated genomes by qPCR

A 20 μL aliquot of each sample was made 10 mM Tris–HCl, pH 8.0, and 6 mM $CaCl_2$, then digested for 1 h at 37 °C with 0.4 mg/mL micrococcal nuclease. EGTA was added to 15 mM to chelate calcium ions and inactivate the nuclease. Samples were then diluted at least 1:100 in TES buffer (1 mM Tris–HCl pH 8.0, 0.1 mM EDTA, 10 μg/mL salmon sperm DNA) before adding 5 μL to a 50 μL qPCR reaction.

This protocol was tested by measuring the genome concentration of plasmid DNA or purified virus, either following straight dilution in TES, or after performing the assay described above with or without the addition of nuclease. There was no significant difference in measured genome concentration for purified virus under any of these conditions, showing that neither the buffer alone nor digestion with nuclease have any effect on accurate measurement of encapsidated genomes. However, while measured plasmid DNA concentration was unaffected by the addition of buffer alone, it was reduced ~10,000 fold in the presence of nuclease.

Measuring encapsidated genomes following multiple- or single-round co-infections

For multiple-round co-infections (performed in the absence of neuraminidase), 100 mm culture dishes were seeded with 300,000 BJ-ELR each, and incubated overnight at 37 °C. Medium was replaced with 900 μL of inoculum containing an equimolar mixture of standard and alternate viruses, each at a concentration of 20 genomes per cell. Plates were incubated at 37 °C for 2 h, then the inoculum was replaced with 10 mL growth medium. At 72 hpi the cells were scraped into the medium, collected by centrifugation, resuspended in TE8.7 and subjected to three freeze–thaw cycles to extract the virus. For each plate, 10% of cell extract was combined with 10% of the supernatant for qPCR analysis, along with a sample of inoculum, as described above. For the second passage of competition, the cell extract/supernatant mixtures generated and measured in the first passage were used as inocula, diluted to a total encapsidated genome concentration of 40 genomes per cell, and treated as before.

For single round coinfections, 35 mm diameter plates were seeded with 100,000 BJ-ELR, incubated overnight at 37 °C, then infected with 200 μL of inoculum containing an equimolar mixture of standard and alternate virus, each at 1000 genomes per cell and incubated at 37 °C. At 4 hpi, one set of plates was harvested, and medium on all other plates was changed to 200 μL of medium containing neuraminidase at 0.1 mg/mL to cleave off viral receptor. At 6 hpi, another set of plates was harvested, and medium on the remaining plates changed to 2 mL of medium containing neuraminidase. These plates were incubated at 37 °C before being harvested at 24 hpi or 48 hpi as described above, except that medium supernatants and cell extracts were analyzed separately.

Analysis of replicative-form DNA

250,000 BJ-ELR were seeded in 60 mm dishes, incubated overnight at 37 °C, then coinfected, under single-round conditions, at 1000 genomes per cell of each virus. Pelleted cells were harvested in 100 μL of Hirt Wash Buffer (20 mM Tris, 150 mM NaCl, 10 mM EDTA), and replicative form DNA isolated by a modification of the method of Hirt extraction as described previously (Tattersall et al., 1973), and half of each sample electrophoresed in a 1.4% agarose gel. For the 24 and 48 hpi samples, gel slices from the 5 kb and 10 kb region of each lane were processed with the QIAquick® Gel Extraction Kit (Qiagen) into 30 μL of 10 mM Tris pH 8.0. 5 μL of each these extracts, in addition to 5 μL of the 6 hpi DNA extract, were directly analyzed by qPCR. The remaining half of each sample was electrophoresed on a separate gel, which was ethidium-stained, photographed, and analyzed by Southern blot using a ^{32}P-labeled probe generated from the PmlI–NarI (NS1 region) fragment of MVM using a Random Primed DNA Labeling Kit (Roche, Indianapolis, IN). An image of the ethidium-stained gel was overlaid in Adobe Photoshop with an image of the Southern blot autoradiograph by aligning vertical and horizontal markers within each.

Statistical analysis

Expansion indices were compared by *t* Test, using KaleideGraph software v3.6 (Synergy Software) after logarithmic conversion of data ($x' = \log(x+1)$) as recommended for statistical analysis of ratios (Ryder and Robakiewicz, 2001).

Acknowledgments

We thank Greg Howe, Jill Crouch, Rex Paternoster and Penny Smith, for assistance with the performance of qPCR, Robert Weinberg for generously providing the BJ-ELR cell line, Orlando Klass for assistance in generating LuCap and LuCap-Alt, and Susan Cotmore for providing pMLM and critically reading the manuscript. This work was funded, in part, by PHS grant number CA029303 from the National Cancer Institute. JCP was funded, in part, by the American Cancer Society High Plains Division—North Texas Postdoctoral Fellowship.

References

Agbandje-McKenna, M., Llamas-Saiz, A.L., Wang, F., Tattersall, P., Rossmann, M.G., 1998. Functional implications of the structure of the murine parvovirus, minute virus of mice. Structure 6, 1369–1381.
Arruda, V.R., Xiao, W., 2007. It's all about the clothing: capsid domination in the adeno-associated viral vector world. J. Thromb. Haemost. 5, 12–15.
Ball-Goodrich, L.J., Tattersall, P., 1992. Two amino acid substitutions within the capsid are coordinately required for acquisition of fibrotropism by the lymphotropic strain of minute virus of mice. J. Virol. 66, 3415–3423.
Chen, Y.Q., de Foresta, F., Hertoghs, J., Avalosse, B.L., Cornelis, J.J., Rommelaere, J., 1986. Selective killing of simian virus 40-transformed human fibroblasts by parvovirus H-1. Cancer Res. 46, 3574–3579.
Chen, Y.Q., Tuynder, M.C., Cornelis, J.J., Boukamp, P., Fusenig, N.E., Rommelaere, J., 1989. Sensitization of human keratinocytes to killing by parvovirus H-1 takes place during their malignant transformation but does not require them to be tumorigenic. Carcinogenesis 10, 163–167.
Cornelis, J.J., Salome, N., Dinsart, C., Rommelaere, J., 2004. Vectors based on autonomous parvoviruses: Novel tools to treat cancer? J. Gene Med. 6 (Suppl 1), S193–S202.
Cotmore, S.F., Tattersall, P., 1992. In vivo resolution of circular plasmids containing concatemer junction fragments from minute virus of mice DNA and their subsequent replication as linear molecules. J. Virol. 66, 420–431.
Cotmore, S.F., Tattersall, P., 2005. Genome packaging sense is controlled by the efficiency of the nick site in the right-end replication origin of parvoviruses minute virus of mice and LuIII. J. Virol. 79, 2287–2300.
Dupont, F., 2003. Risk assessment of the use of autonomous parvovirus-based vectors. Curr. Gene Ther. 3, 567–582.
Dupont, F., Avalosse, B., Karim, A., Mine, N., Bosseler, M., Maron, A., Van den Broeke, A., Ghanem, G.E., Burny, A., Zeicher, M., 2000. Tumor-selective gene transduction and cell killing with an oncotropic autonomous parvovirus-based vector. Gene Ther. 7, 790–796.
Dupressoir, T., Vanacker, J.M., Cornelis, J.J., Duponchel, N., Rommelaere, J., 1989. Inhibition by parvovirus H-1 of the formation of tumors in nude mice and colonies in vitro by transformed human mammary epithelial cells. Cancer Res. 49, 3203–3208.
Everts, B., van der Poel, H.G., 2005. Replication-selective oncolytic viruses in the treatment of cancer. Cancer Gene Ther. 12, 141–161.
Faisst, S., Guittard, D., Benner, A., Cesbron, J.Y., Schlehofer, J.R., Rommelaere, J., Dupressoir, T., 1998. Dose-dependent regression of HeLa cell-derived tumours in SCID mice after parvovirus H-1 infection. Int. J. Cancer 75, 584–589.
Farr, G.A., Cotmore, S.F., Tattersall, P., 2006. VP2 cleavage and the leucine ring at the base of the fivefold cylinder control pH-dependent externalization of both the VP1 N terminus and the genome of minute virus of mice. J. Virol. 80, 161–171.
Farr, G.A., Tattersall, P., 2004. A conserved leucine that constricts the pore through the capsid fivefold cylinder plays a central role in parvoviral infection. Virology 323, 243–256.
Farr, G.A., Zhang, L.G., Tattersall, P., 2005. Parvoviral virions deploy a capsid-tethered lipolytic enzyme to breach the endosomal membrane during cell entry. Proc. Natl. Acad. Sci. U. S. A. 102, 17148–17153.
Gardiner, E.M., Tattersall, P., 1988a. Evidence that developmentally regulated control of gene expression by a parvoviral allotropic determinant is particle mediated. J. Virol. 62, 1713–1722.
Gardiner, E.M., Tattersall, P., 1988b. Mapping of the fibrotropic and lymphotropic host range determinants of the parvovirus minute virus of mice. J. Virol. 62, 2605–2613.

Garnick, R.L., 1996. Experience with viral contamination in cell culture. Dev. Biol. Stand. 88, 49–56.
Geletneky, K., Kiprianova, I., Ayache, A., Koch, R., Herrero, Y., Calle, M., Deleu, L., Sommer, C., Thomas, N., Rommelaers, J., Schlehofer, J.R., 2010. Regression of advanced rat and human gliomas by local or systemic treatment with oncolytic parvovirus H-1 in rat models. Neuro Oncol. 12, 804–814.
Guetta, E., Graziani, Y., Tal, J., 1986. Suppression of ehrlich ascites tumors in mice by minute virus of mice. J. Natl. Cancer Inst. 76, 1177–1180.
Guetta, E., Mincberg, M., Mousset, S., Bertinchamps, C., Rommelaere, J., Tal, J., 1990. Selective killing of transformed rat cells by minute virus of mice does not require infectious virus production. J. Virol. 64, 458–462.
Hahn, W.C., Counter, C.M., Lundberg, A.S., Beijersbergen, R.L., Brooks, M.W., Weinberg, R.A., 1999. Creation of human tumour cells with defined genetic elements. Nature 400, 464–468.
Hahn, W.C., Weinberg, R.A., 2002. Modelling the molecular circuitry of cancer. Nat. Rev. Cancer 2, 331–341.
Hallauer, C., Siegl, G., Kronauer, G., 1972. Parvoviruses as contaminants of permanent human cell lines. 3. Biological properties of the isolated viruses. Arch. Gesamte. Virusforsch. 38, 366–382.
Hirt, B., 1967. Selective extraction of polyoma DNA from infected mouse cell cultures. J. Mol. Biol. 26, 365–369.
Legrand, C., Mousset, S., Salome, N., Rommelaere, J., 1992. Cooperation of oncogenes in cell transformation and sensitization to killing by the parvovirus minute virus of mice. J. Gen. Virol. 73, 2003–2009.
Maxwell, I.H., Spitzer, A.L., Maxwell, F., Pintel, D.J., 1995. The capsid determinant of fibrotropism for the MVMp strain of minute virus of mice functions via VP2 and not VP1. J. Virol. 69, 5829–5832.
Maroto, B., Valle, N., Saffrich, R., Almendral, J.M., 2004. Nuclear export of the nonenveloped parvovirus virion is directed by an unordered protein signal exposed on the capsid surface. J. Virol. 78, 10685–10694.
Mousset, S., Ouadrhiri, Y., Caillet-Fauquet, P., Rommelaere, J., 1994. The cytotoxicity of the autonomous parvovirus minute virus of mice nonstructural proteins in FR3T3 rat cells depends on oncogene expression. J. Virol. 68, 6446–6453.
Nam, H.J., Gurda-Whitaker, B., Gan, W.Y., Ilaria, S., McKenna, R., Mehta, P., Alvarez, R.A., Agbandje-McKenna, M., 2006. Identification of the sialic acid structures recognized by minute virus of mice and the role of binding affinity in virulence adaptation. J. Biol. Chem. 281, 25670–25677.
Previsani, N., Fontana, S., Hirt, B., Beard, P., 1997. Growth of the parvovirus minute virus of mice MVMp3 in EL4 lymphocytes is restricted after cell entry and before viral DNA amplification: cell-specific differences in virus uncoating in vitro. J. Virol. 71, 7769–7780.
Raykov, Z., Grekova, S., Galabov, A.S., Balboni, G., Koch, U., Aprahamian, M., Rommelaere, J., 2007. Combined oncolytic and vaccination activities of parvovirus H-1 in a metastatic tumor model. Oncol. Rep. 17, 1493–1499.
Rommelaere, J., Cornelis, J.J., 1991. Antineoplastic activity of parvoviruses. J. Virol. Methods 33, 233–251.
Ryder, E.F., Robakiewicz, P., 2001. Statistics for the molecular biologists: group comparisons. Curr. Protoc. Mol. Biol. A.3I.1–A.3I.22.
Shi, Z.Y., Ma, C.W., Huang, J., Lin, W.M., Dong, R.C., Luo, Z.Y., 1997. Inhibition of parvovirus H-1 on transplantable human hepatoma and its histological and histobiochemical studies. Shi Yan Sheng Wu Xue Bao 30, 247–259.
Siegl, G., 1984. The parvoviruses. In: Bern, K.I. (Ed.), Biology and pathogenicity of autonomous parvoviruses. Plenum Press, New York, pp. 297–362.
Spalholz, B.A., Tattersall, P., 1983. Interaction of minute virus of mice with differentiated cells: strain-dependent target cell specificity is mediated by intracellular factors. J. Virol. 46, 937–943.
Tattersall, P., Crawford, L.V., Shatkin, A.J., 1973. Replication of the parvovirus MVM. II. Isolation and characterization of intermediates in the replication of the viral deoxyribonucleic acid. J. Virol. 12, 1446–1456.
Tattersall, P., Bratton, J., 1983. Reciprocal productive and restrictive virus–cell interactions of immunosuppressive and prototype strains of minute virus of mice. J. Virol. 46, 944–955.
Tattersall, P., Bergoin, M., Bloom, M.E., Brown, K.E., Linden, R.M., Muzyczka, N., Parrish, C.R., Tijssen, P., 2005. Parvoviridae. In: Fauquet, C.M., Mayo, M.A., Maniloff, J., Desselberger, U., Ball, L.A. (Eds.), Virus Taxonomy, VIIIth Report of the ICTV. Elsevier/Academic Press, London, pp. 593–608.
Toolan, H.W., 1967. Lack of oncogenic effect of the H-viruses for hamsters. Nature 214, 1036.
Toolan, H.W., Rhode III, S.L., Gierthy, J.F., 1982. Inhibition of 7,12-dimethyl-benz(a) anthracene-induced tumors in syrian hamsters by prior infection with H-1 parvovirus. Cancer Res. 42, 2552–2555.
Van Hille, B., Duponchel, N., Salome, N., Spruyt, N., Cotmore, S.F., Tattersall, P., Cornelis, J.J., Rommelaere, J., 1989. Limitations to the expression of parvoviral nonstructural proteins may determine the extent of sensitization of EJ-ras-transformed rat cells to minute virus of mice. Virology 171, 89–97.
Van Vliet, K.M., Blouin, V., Brument, N., Agbandje-McKenna, M., Snyder, R.O., 2008. The role of the adeno-associated virus capsid in gene transfer methods. Mol. Biol. 437, 51–91.
Wrzesinski, C., Tesfay, L., Salome, N., Jauniaux, J.C., Rommelaere, J., Cornelis, J., Dinsart, C., 2003. Chimeric and pseudotyped parvoviruses minimize the contamination of recombinant stocks with replication-competent viruses and identify a DNA sequence that restricts parvovirus H-1 in mouse cells. J. Virol. 77, 3851–3858.
Wu, J.T., Byrne, H.M., Kirn, D.H., Wein, L.M., 2001. Modeling and analysis of a virus that replicates selectively in tumor cells. Bull. Math. Biol. 63, 731–768.